UNIVERSITY OF BIRMINGHAM

University of Birmingham
Research at Birmingham

Finite-temperature effects on the x-ray absorption spectra of crystalline alumina from first principles

Harper, A. F.; Monserrat, B.; Morris, A. J.

Document Version
Publisher's PDF, also known as Version of record

[Link to publication on Research at Birmingham portal](#)

Finite-temperature effects on the x-ray absorption spectra of crystalline alumina from first principles

A. F. Harper ; B. Monserrat ; A. J. Morris

Check for updates

View Online   Export Citation   CrossMark

Finite-temperature effects on the x-ray absorption spectra of crystalline alumina from first principles

View Online   Export Citation   CrossMark

A. F. Harper,[1] (ID) B. Monserrat[2] (ID) and A. J. Morris[3,a] (ID)

AFFILIATIONS

[1] Theory of Condensed Matter, Cavendish Laboratory, University of Cambridge, J. J. Thomson Avenue, Cambridge CB3 0HE, United Kingdom
[2] Department of Materials Science and Metallurgy, University of Cambridge, 27 Charles Babbage Road, Cambridge CB3 0FS, United Kingdom
[3] School of Metallurgy and Materials, University of Birmingham, Edgbaston, Birmingham B15 2TT, United Kingdom

[a] Author to whom correspondence should be addressed: a.j.morris.1@bham.ac.uk

ABSTRACT

By including phonon-assisted transitions within plane-wave density functional theory methods for calculating the x-ray absorption spectrum (XAS), we obtain the Al K-edge XAS at 300 K for two crystalline Al_2O_3 phases. The 300 K XAS reproduces the pre-edge peak for α-Al_2O_3, which is not visible at the static lattice level of approximation. Configurations from Monte Carlo sampling of the γ-Al_2O_3 phase space at the 300 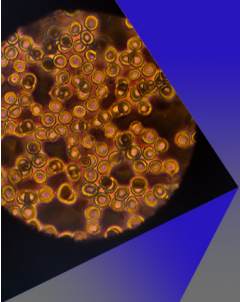K XAS correctly describe two out of the three experimental peaks. We show that the second peak arises from 1s to mixed s-p transitions and is absent in the 0 K XAS. This letter serves as an insight into the electronic origins of the characteristic peaks in the Al K-edge XAS for alumina crystals.

I. INTRODUCTION

Crystalline phases of alumina have a range of applications in ceramic and abrasive manufacturing.[1–3] Given the breadth of the literature, especially in the case of corundum (the low energy α-alumina phase), the crystal structure of α-alumina may be deemed well-characterized by both experimental and computational methods. As alumina are increasingly used in electronic applications such as perovskite solar cells and heterogeneous catalysts,[4–6] it has become imperative to understand not only their atomistic but also their electronic structure, especially in the less well characterized phases such as γ-Al_2O_3. X-ray absorption spectroscopy methods have been used to obtain the K-edge absorption spectra for α-alumina[7] and, more recently, for γ-alumina,[8] providing experimental insight into the electronic structure of these materials.

The Al K-edge XAS for α-Al_2O_3[9] has a main absorption peak at 1568 eV, which accounts for transitions to 3p states in the conduction band. Full multiple-scattering calculations reproduced this main peak but failed to capture the pre-edge predicted to arise from dipole-forbidden transitions from Al 1s to 3s states.[10] The pre-edge was later described using first-principles calculations which introduced the effect of atomic vibrations into the absorption cross section, with a method designed for cases in which the vibrational energies are small in relation to the absorption energy (as is the case for Al).[11] This confirmed that the existence of the pre-edge was allowed due to s-p mixing arising from distortions with the local AlO_6 environment.[12] However, this approximation assumes that the final electronic state of the system is not affected by vibrational modes and therefore calculates the excited electronic state without any vibrational effects included. Furthermore, as is shown for the case of Ti,[11] this method is unable to reproduce transitions between the Ti s and d states as the assumption that the vibrational energies are small relative to the absorption energies no longer holds. While this approximation works for localized, small energy effect transitions, it is not generally applicable.

Incorporating vibrational effects using configurational averaging across first-principles calculations to obtain temperature

09 August 2023 09:40:16

dependent spectroscopy is the state-of-the-art. For example, finite-temperature nuclear magnetic resonance chemical shifts were compared within 2–4 ppm of the experimental results for both organic[13] and inorganic[14] solid-state systems. Finite-temperature XAS of the Mg K-edge of MgO has also been studied, and a correlation between increasing temperature and decreasing absorption energy of the pre-edge peak was found in the Mg K-edge.[14] The temperature dependent K-edge XAS of light elements and oxides, including α-Al$_2$O$_3$, was reported by Nemausat et al.,[15] and we compare their results at 300 K to those presented in our work herein.

In this letter, we use first-principles XAS calculations combined with phonon calculations to produce the Al K-edge XAS at 300 K of both α- and γ-alumina. By incorporating these effects at 300 K, we are able to fully describe the pre-edge peak in α-alumina. In addition, we calculate the Al K-edge XAS spectra for γ-alumina and assign both structural and electronic features to two of the three main edges in the γ-alumina XAS. We examine the electronic charge density of the third peak in the spectrum and propose that this peak is attributed to delocalized d-like states. This method of calculating finite-temperature XAS using first-principles accuracy can be similarly used on other crystalline structures, and this method provides an example of the utility of incorporating phonon effects in the modeling of the XAS.

II. THEORY AND COMPUTATIONAL DETAILS

The XAS measures the electronic transitions from a core state (in this case the Al $1s$ state for the Al K-edge spectrum) to the excited states in the conduction band of the material. The transitions are short range and vertical and normally describe differences in the energy states between nearest-neighbor atoms. When using pseudopotential plane-wave density-functional theory (DFT), which does not explicitly treat electrons in the core orbitals, it is necessary to approximate the effect of the x-ray excitation of an electron by incorporating a pseudopotential at the site of the excitation, which has the electronic configuration of the atom with an electron removed from the core state.[16] This core-hole pseudopotential method has shown success in reproducing the experimental absorption spectra of a range of materials,[17–19] as implemented in the DFT code CASTEP.[20] To recover the wave function of the all-electron core state requires a transformation using a projector-augmented wave approach, in which each transmission matrix element is calculated from a linear transformation of the pseudo wavefunction.[16]

The x-ray absorption cross section, σ, is described using Fermi's golden rule approximation to the imaginary part of the dielectric function,[14,21]

$$\sigma(\omega) = 4\pi^2 \alpha_0 \hbar \omega \sum_f \left| \langle \Psi_f | \hat{\boldsymbol{\epsilon}} \cdot \mathbf{r} | \Psi_i \rangle \right|^2 \delta(E_f - E_i - \hbar\omega), \quad (1)$$

where $\hbar\omega$ is the energy of the incoming x ray, $\mathbf{r}$ is the single electron position operator, α_0 is the fine structure constant, and $\hat{\boldsymbol{\epsilon}}$ is the polarization direction of the electromagnetic vector potential. The incoming x ray excites an electron from a core-level orbital $|\Psi_i\rangle$ to a final state $|\Psi_f\rangle$ in the conduction band. The final electronic states, $|\Psi_f\rangle$, are eigenstates of the Kohn–Sham Hamiltonian.

The zero temperature approximation of the x-ray absorption cross section [Eq. (1)] can be extended to finite-temperature

using the Williams-Lax theory,[14,22–24] which yields the following expression:

$$\sigma(T) = \frac{1}{\mathbb{Z}} \sum_k \langle \chi_k(\mathbf{R}) | \sigma(\omega, \mathbf{R}) | \chi_k(\mathbf{R}) \rangle e^{-E_k/k_B T}, \quad (2)$$

in which $\mathbb{Z} = \sum_k e^{-E_k/k_B T}$ is the partition function from the initial state, where E_k is the energy of vibrational state k and $|\chi_k(\mathbf{R})\rangle$ is the vibrational wave function with nuclear configuration $\mathbf{R}$, which we describe within the harmonic approximation in this letter. Using a Monte Carlo (MC) sampling technique, described in detail in Ref. 24, we evaluate Eq. (2) by calculating a series of x-ray absorption transition energies for sampled nuclear configurations $\mathbf{R}$ distributed according to the harmonic vibrational density.

III. RESULTS

A. α-Al$_2$O$_3$

The experimental Al K-edge absorption spectrum for α-Al$_2$O$_3$ contains three peaks (**a**, **b**, and **c**) at 1565, 1568, and 1572 eV, respectively, shown in Fig. 1. The pre-edge peak at **a** is assigned to transitions from Al $1s$ to $3s$ states.[8] At 1568 eV, peak **b** is the main absorption peak in the Al octahedral sites and results from a transition from the Al $1s$ to $3p$ state. Peak **c** is attributed to transitions from the Al $1s$ to $3d$ states.[8]

The ground-state static lattice XAS calculation of α-Al$_2$O$_3$ reproduces peaks **b** and **c** (Fig. S3a), but the pre-edge at **a** is absent. This pre-edge comprises an s-to-s transition; hence, it is dipole forbidden due to the octahedral symmetry present in the unit cell. However, the pre-edge peak at **a**, as well as peaks **b** and **c**, is visible in the XAS calculated at 300 K, indicating that the inclusion
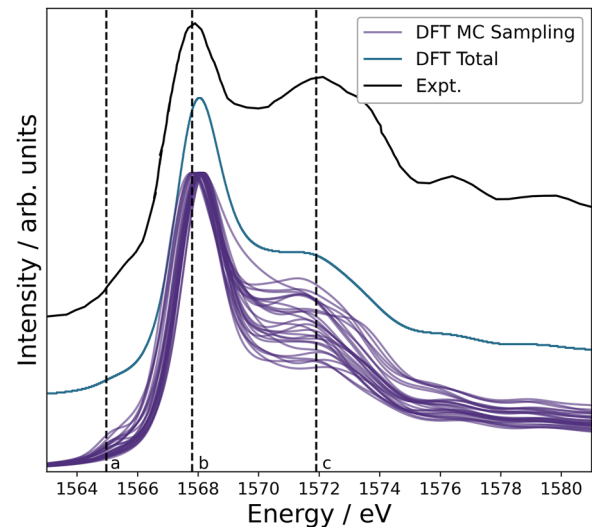
FIG. 1. XAS at 300 K (blue) calculated as a sum of 30 spectra from the MC sampled configurations of α-Al2O3 (purple) compared to the experimental XAS from the study by Cabaret and Brouder,[12] indicating that the pre-peak at **a** is visible in the MC sampled spectra. Experimental spectrum adapted with permission from D. Cabaret and C. Brouder, J. Phys.: Conf. Ser. **190**, 012003 (2009). Copyright 2009 IOP Publishing; licensed under a Creative Commons Attribution (CC BY) license.

of phonon assisted transitions successfully describes all three peaks in the α-Al_2O_3 Al K-edge XAS. These results are consistent with the Al K-edge spectrum calculated by Nemausat[15] at 300 K, which matches peaks **a**, **b**, and **c** with the experimental spectrum. In addition, they show at increasing temperatures that the intensity of peak **a** increases, suggesting that with increasing temperature and local disorder, there are additional allowed transitions due to the vibration-induced symmetry breaking; this trend is present both in the experiment and in first principles calculations.

One major benefit of calculating spectral features with DFT is the direct access to the electronic structure of the material; thus, we go one step beyond calculating the spectrum and explore the band character of the transitions at pre-edge peak **a**. By calculating the electronic density of states (DOS) for both the ground-state static lattice case and a configuration from the MC sampling, we can determine the orbital character of the pre-edge states. In both the ground-state static lattice and MC sampling configuration DOS, there are Al 3s states at 3 eV above the Fermi level; however, in the MC sampling case, there are additional Al 3s states at this energy level. The presence of the additional Al 3s states is a result of the distortion of the lattice at 300 K breaking the inversion symmetry of the cell and allowing s-to-s transitions. This additionally distorts the electron density and local octahedral environment surrounding the Al atom (shown in Fig. 2, right). Thus, while the Al 3s states are present in both cases, the transitions at the pre-edge are allowed only in the MC sampled configuration due to the breaking of local symmetry.

B. γ-Al_2O_3

The Al K-edge XAS spectrum for γ-alumina is less well-understood than that of α-Al_2O_3 despite the large number of studies on the K-edge spectrum of aluminosilicate glasses.[25–27] Unlike
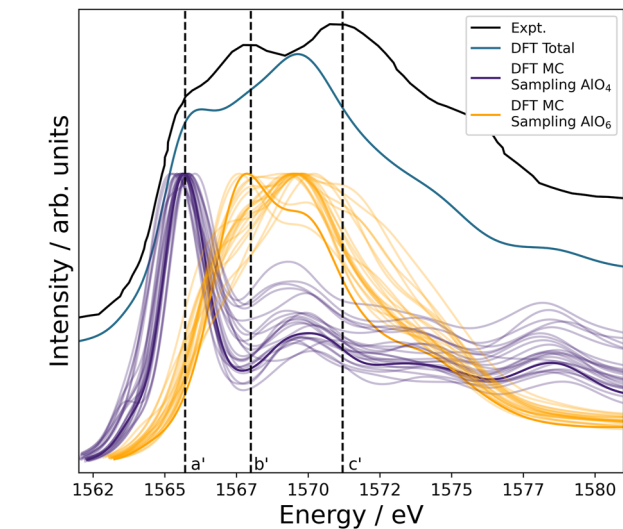
FIG. 3. XAS at 300 K for γ-Al_2O_3 calculated as the weighted average over 30 generated configurations from Monte Carlo sampling over the static lattice phonon modes. Peak **a′** described the spectra with a core-hole on the AlO_4 site well. Peak **b′** is described by six spectra with a core-hole on the AlO_6 site, and the remaining spectra with a core-hole on the AlO_6 site have a peak at 1570.0 eV. Only the **c′** peak from the experiment is not described by the spectrum at 300 K. Experimental spectrum adapted with permission from Altman et al., Inorg. Chem. **56**, 5710–5719 (2017). Copyright 2017 American Chemical Society.

α-alumina, which contains only one, symmetry-equivalent, octahedral AlO_6 site, in the γ-Al_2O_3 phase, there are two symmetry-inequivalent sites—an octahedral AlO_6 site and tetrahedral AlO_4 site. The cation disorder in this system has led to several model unit cells of γ-alumina.[28] Discrepancies between experimental x-ray
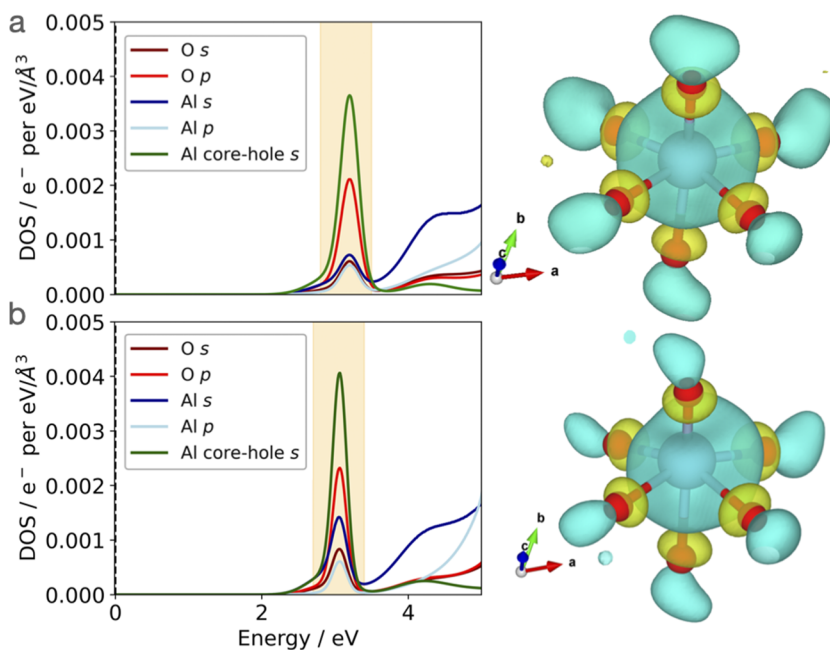
FIG. 2. (a) Electronic DOS for the ground-state static lattice structure of α-Al_2O_3 and visualization of the states at 3 eV surrounding the core-hole Al atom. (b) Electronic DOS and visualization for one MC sampling configuration of α-Al_2O_3. The orange shaded region in the DOS is the energy at which the electron density is calculated. In the right panels, Al atoms are shown in blue, O atoms are shown in red, and the positive (blue) and negative (yellow) electron densities are shown in 3D.

diffraction and first principles models suggest a variety of potential models for γ-Al_2O_3, namely, a spinel model in which the Al^{3+} cations are all on spinel sites,[29] a spinel model in which these cations sit on non-spinel sites,[30] and a non-spinel model.[31,32] In this work, we have chosen to use Pinto et al., phase of γ-Al_2O_3[30] as the recent selected-area electron diffraction analysis suggests that Pinto et al., model shows excellent agreement with the experiment.[28,33]

The presence of two symmetry-inequivalent sites in γ-Al_2O_3 requires careful treatment of the contribution of these two sites to the overall XAS lineshape. Typically, the total XAS spectra are weighted according to the abundance of each symmetry-inequivalent atom in the system;[34] thus, to calculate the γ-Al_2O_3 XAS, we weight the contribution of core-holes placed on AlO_4 and AlO_6 sites according to their abundance in the static lattice unit cell (10 AlO_6 to 6 AlO_4 units).

The experimental Al K-edge XAS of γ-Al_2O_3 contains an edge (**a′**) at 1565.7 eV and two peaks (**b′** and **c′**) at 1568.0 and 1571.2 eV, respectively. Edge **a′** and peak **b′** have been assigned to $1s$ to $3p$ transitions, and **c′** is assigned to $1s$ to $3d$ transitions.[8] Peak **c′** at 1571.2 eV is also present in the α-Al_2O_3 XAS and other aluminosilicate materials, corresponding to transitions to Al $3d$ states.[8] The ground-state static lattice XAS with a core-hole placed on the AlO_4 site reproduces the peak at **a′**, but the XAS with a core-hole placed on the AlO_6 site has a peak with an absorption energy between **b′** and **c′** at 1570.0 eV. Overall, the static lattice XAS (Figure S3b) describes neither peak **b′** or **c′**.

At 300 K, the first principles XAS for γ-Al_2O_3 has peaks at 1565.7 and 1570.0 eV, as shown in Fig. 3. The peak at 1565.7 eV corresponds to **a′** in the experiment. The XAS at 300 K successfully reproduces peak **b′** at 1568.0 eV in a set of 6 MC sampled
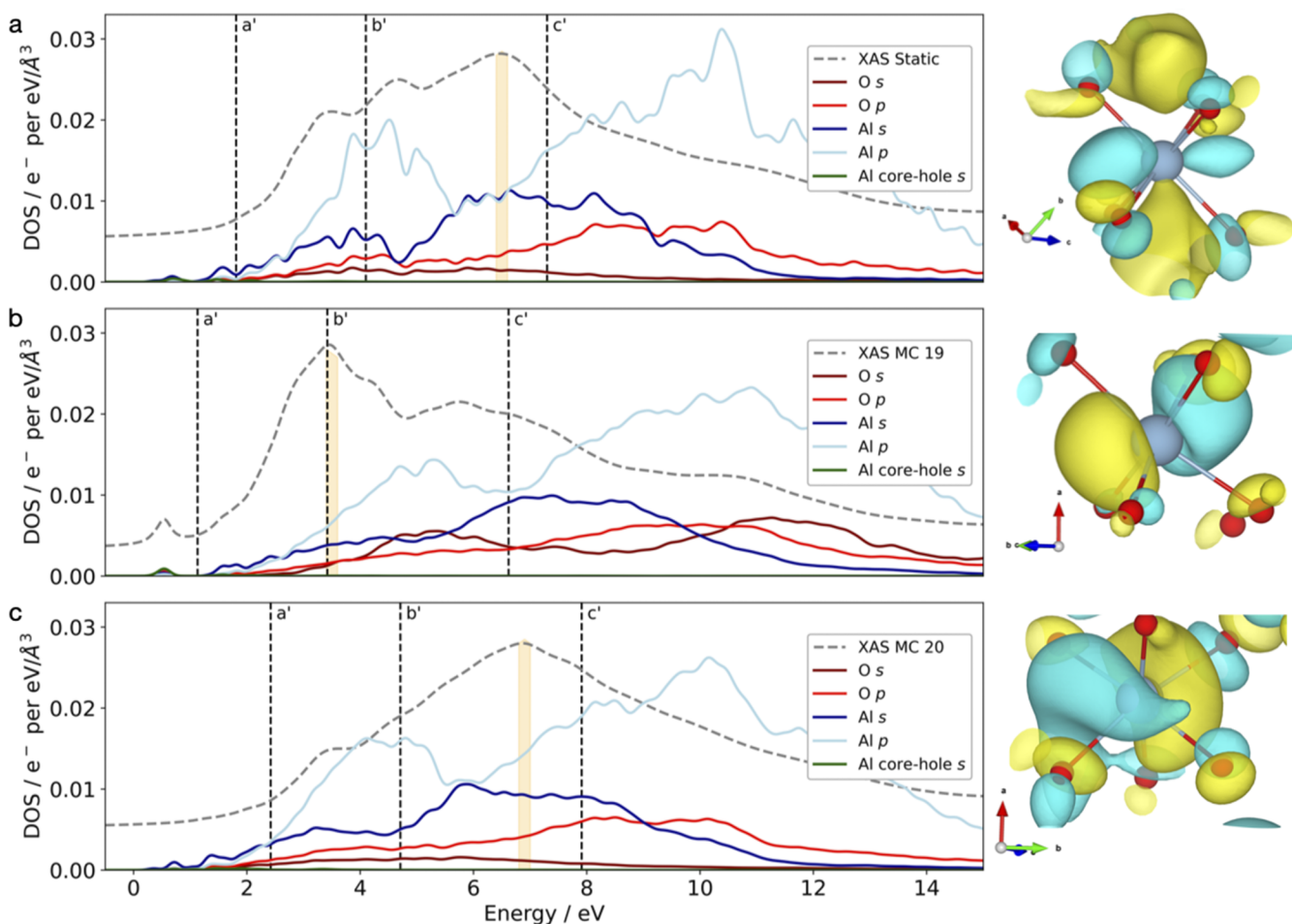
FIG. 4. Electronic DOS for the static lattice structure of γ-Al_2O_3 (a) and two configurations from MC sampling at 300 K [(b) and (c)] alongside the orbital character of the states giving rise to the main peak in the XAS for each case. The Fermi level is at 0 eV, and the XAS is aligned to the corresponding energy levels in the DOS. The orange shaded region in the DOS is the point at which the electron density is calculated. In the right panels, Al atoms are shown in blue, O atoms are shown in red, and the positive (blue) and negative (yellow) electron densities are shown in 3D. (a) Electronic DOS for the static lattice structure of γ-Al_2O_3 and visualization of the Al d-like states giving rise to the maximum between **b′** and **c′** in the XAS. (b) Electronic DOS for MC sampling configuration 19 and visualization of mixed s-p states corresponding to a maximum peak in the XAS of 1568.0 eV at **b′**. (c) Electronic DOS for MC sampling configuration 20 and visualization of delocalized electronic orbitals that cannot easily be assigned to s, p, or d characters, corresponding to an XAS peak at 1570.0 eV between **b′** and **c′**.

configurations with a core-hole on the AlO$_6$ site. This peak is not described by the static lattice XAS for γ-Al$_2$O$_3$ shown in Fig. S3, highlighting the need for incorporating temperature effects. Finally, the third peak in the XAS at 300 K is 1.2 eV lower than the **c′** transition and is present in a set of 24 MC configurations with a core-hole placed on the AlO$_6$ site.

To determine the band character of the states that give rise to each peak in the XAS, we compare the static lattice DOS [shown in Fig. 4(a)] with the electronic DOS from an MC configuration that reproduces peak **b′** [shown in Fig. 4(b)] and one that reproduces the peak at 1570.0 eV [shown in Fig. 4(c)]. In the ground-state static lattice unit cell with a core-hole placed on the AlO$_6$ site, shown in Fig. 4(a), the electron density at the 1570.0 eV peak in the XAS visually appears to have a d-like character; however, the distortion at this site results in assignment of the Als or Alp character in DFT (6.5 eV above the Fermi level in the DOS).

The electronic DOS for one MC sampling configuration, shown in Fig. 4(b), with a peak at **b′**, shows that the states at **b′** have a mixed s-p character. This peak has previously been assigned to Al 1s to 3p states;[8] however, these results suggest that the orbital character of these states is mixed s-p. Figure 4(c) also shows the DOS for a configuration from MC sampling, which has a peak at 1570.0 eV in the XAS. The states that contribute to the peak at 1570.0 eV are delocalized in real space and therefore are not easily assigned to an s, p, or d character when computing the projection onto atomic orbitals.

Peak **c′** in the XAS shown in Fig. 3 is not described by any of the spectra with core-holes placed on the AlO$_6$ site in the MC configurations at 300 K. However, the distorted d-like states in the static lattice spectrum shown in Fig. 4(a), as well as the delocalized states in the configuration from MC sampling in 4c, are suggestive of transitions to d-like states, as in the experiment at peak **c′**. Although the DFT transition energy of this third peak is at a lower energy than in the experiment, this is a good first approximation for visualizing these mixed states at peak **c′**. One potential source of this discrepancy is in the use of the Perdew–Burke–Ernzerhof (PBE) functional and could be resolved through an investigation of the electronic states in the region above the Fermi level using a hybrid functional. While this is beyond the scope of this work, which focuses on the DOS, this could resolve the energy difference between the **c′** experiment and theory. Using a multiple-scattering approach to calculate the XAS would resolve features at higher energies; however, our work here determines which transitions are a function of thermal vibrations and obtain accurate transition energies near the absorption edge using DFT. However, given the strong agreement between theory and experiment for peaks **a′** and **b′**, there is reason to suggest that the structure is the source of this energy difference. By calculating the XAS of another γ-Al$_2$O$_3$ structure, one could explore the effects of partial occupancy on the electronic configurations.

IV. CONCLUSIONS

Monte-Carlo sampling of the vibrational modes of the ground state structure of both α- and γ-Al$_2$O$_3$ has shed light on the origins of their electronic transitions in the XAS and suggested possible further studies for γ-Al$_2$O$_3$. The XAS at 300 K for α-Al$_2$O$_3$ is in agreement with previous results[15] and accurately reproduces the absorption pre-edge not observed at the static lattice level of theory; in addition,

the resulting electronic states above the Fermi level show s-p mixing. The ground state XAS for γ-Al$_2$O$_3$ only describes the K-edge transitions in the AlO$_4$ sites. By incorporating finite-temperature effects, we are able reproduce two of three peaks in the experimental Al K-edge XAS using individual configurations from MC sampling.

Using the Williams-Lax theory together with a stochastic configuration sampling technique[15,22–24] is a general method for calculating the finite-temperature XAS. By calculating the corresponding DOS for each spectrum, we gain additional information, which is not accessible in the experiment, including visualizing the electronic charge density alongside the corresponding absorption peaks. Thus, the XAS calculated at 300 K for α- and γ-Al$_2$O$_3$ not only contains the same peak positions but also the same assigned orbital transitions as the experiment. In order to calculate L$_1$ or L$_{2,3}$ absorption edges, further approximations are needed, such as multiple scattering Green's function's approaches[35] or linear response methods.[36] The multiple scattering approach has previously been combined with DFT-calculated forces to calculate finite temperature Debye–Waller factors,[37] and the methods presented in this paper could be modified in a similar fashion to incorporate DFT-calculated vibrational modes. However, additional approximations are needed to calculate especially high temperature spectra, as shown by Laraia et al.[38] Nevertheless, the method presented herein is not specific to crystalline alumina, the Al K-edge absorption spectrum, or x-ray absorption spectroscopy; indeed, it is a general approach for incorporating DFT-calculated forces into a spectroscopic calculation, which can be applied to other systems to study the experimental features not observed at the ground-state static lattice level.

SUPPLEMENTARY MATERIAL

The supplementary material contains five figures which contribute to the understanding of both the methods and results of this work, and the figure captions describe their relevance to the work in the main text. In addition, detailed information about the specific parameters used to calculate the phonons, XAS spectra, and eDOS are also included.

09 August 2023 09:40:16

AUTHOR DECLARATIONS

Conflict of Interest

The authors have no conflicts to disclose.

Author Contributions

A. F. Harper: Conceptualization (equal); Data curation (equal); Formal analysis (equal); Writing – original draft (equal). **B. Monserrat**: Resources (equal); Software (equal); Supervision (equal); Writing – review & editing (equal). **A. J. Morris**: Conceptualization (equal); Funding acquisition (equal); Project administration (equal); Resources (equal); Supervision (equal); Writing – review & editing (equal).

DATA AVAILABILITY

The data that support the findings of this study are openly available in Apollo, the University of Cambridge Data Repository.[39]

REFERENCES

[1] E. Medvedovski, Ceram. Int. **32**, 369 (2006).

[2] R. R. Rao, L. Mariappan, and H. N. Roopa, Procedia Mater. Sci. **5**, 2595 (2014).

[3] K. Y. Paranjpe, Pharma Innovation **6**, 236 (2017).

[4] M. Trueba and S. P. Trasatti, Eur. J. Inorg. Chem. **2005**, 3393.

[5] W. Li, J. Li, L. Wang, G. Niu, R. Gao, and Y. Qiu, J. Mater. Chem. A **1**, 11735 (2013).

[6] C. Das, M. Kot, T. Hellmann, C. Wittich, E. Mankel, I. Zimmermann, D. Schmeisser, M. K. Nazeeruddin, and W. Jaegermann, Cell Rep. Phys. Sci. **1**, 100112 (2020).

[7] Y. Kato, K.-i. Shimizu, N. Matsushita, T. Yoshida, H. Yoshida, A. Satsuma, and T. Hattori, Phys. Chem. Chem. Phys. **3**, 1925 (2001).

[8] A. B. Altman, C. D. Pemmaraju, S. Alayoglu, J. Arnold, C. H. Booth, A. Braun, C. E. Bunker, A. Herve, S. G. Minasian, D. Prendergast *et al.*, Inorg. Chem. **56**, 5710 (2017).

[9] D. Cabaret, P. Sainctavit, P. Ildefonse, and A.-M. Flank, J. Phys.: Condens. Matter **8**, 3691 (1996).

[10] D. Li, G. M. Bancroft, M. E. Fleet, X. H. Feng, and Y. Pan, Am. Mineral. **80**, 432 (1995).

[11] C. Brouder, D. Cabaret, A. Juhin, and P. Sainctavit, Phys. Rev. B **81**, 115125 (2010).

[12] D. Cabaret and C. Brouder, J. Phys.: Conf. Ser. **190**, 012003 (2009).

[13] B. Monserrat, R. J. Needs, and C. J. Pickard, J. Chem. Phys. **141**, 134113 (2014).

[14] R. Nemausat, D. Cabaret, C. Gervais, C. Brouder, N. Trcera, A. Bordage, I. Errea, and F. Mauri, Phys. Rev. B **92**, 144310 (2015).

[15] R. Nemausat, C. Gervais, C. Brouder, N. Trcera, A. Bordage, C. Coelho-Diogo, P. Florian, A. Rakhmatullin, I. Errea, L. Paulatto, M. Lazzeri, and D. Cabaret, Phys. Chem. Chem. Phys. **19**, 6246 (2017).

[16] S.-P. Gao, C. J. Pickard, A. Perlov, and V. Milman, J. Phys.: Condens. Matter **21**, 104203 (2009).

[17] T. Mizoguchi, I. Tanaka, S.-P. Gao, and C. J. Pickard, J. Phys.: Condens. Matter **21**, 104204 (2009).

[18] T. Yamamoto, T. Mizoguchi, K. Tatsumi, I. Tanaka, H. Adachi, Y. Muramatsu, E. M. Gullikson, and R. C. C. Perera, Mater. Trans. **45**, 1991 (2004).

[19] D. Cabaret, F. Mauri, and G. S. Henderson, Phys. Rev. B **75**, 184205 (2007).

[20] S. J. Clark, M. D. Segall, C. J. Pickard, P. J. Hasnip, M. I. J. Probert, K. Refson, and M. C. Payne, Z. Kristallogr. **220**, 567 (2005).

[21] E. Fermi, *Nuclear Physics: A Course Given by Enrico Fermi at the University of Chicago* (University of Chicago Press, 1950).

[22] F. E. Williams, Phys. Rev. **82**, 281 (1951).

[23] M. Lax, J. Chem. Phys. **20**, 1752 (1952).

[24] B. Monserrat, J. Phys.: Condens. Matter **30**, 083001 (2018).

[25] S. De Wispelaere, D. Cabaret, C. Levelut, S. Rossano, A.-M. Flank, P. Parent, and F. Farges, Chem. Geol. **213**, 63 (2004).

[26] D. R. Neuville, L. Cormier, and D. Massiot, Geochim. Cosmochim. Acta **68**, 5071 (2004).

[27] D. R. Neuville, L. Cormier, A.-M. Flank, V. Briois, and D. Massiot, Chem. Geol. **213**, 153 (2004).

[28] H. O. Ayoola, S. D. House, C. S. Bonifacio, K. Kisslinger, W. A. Saidi, and J. C. Yang, Acta Mater. **182**, 257 (2020).

[29] L. Smrčok, V. Langer, and J. Křest'an, Acta Crystallogr., Sect. C **62**, i83 (2006).

[30] H. P. Pinto, R. M. Nieminen, and S. D. Elliott, Phys. Rev. B **70**, 125402 (2004).

[31] M. Digne, P. Sautet, P. Raybaud, P. Euzen, and H. Toulhoat, J. Catal. **226**, 54 (2004).

[32] G. Paglia, C. E. Buckley, A. L. Rohl, B. A. Hunter, R. D. Hart, J. V. Hanna, and L. T. Byrne, Phys. Rev. B **68**, 144110 (2003).

[33] R. Prins, J. Catal. **392**, 336 (2020).

[34] B. P. Klein, S. J. Hall, and R. J. Maurer, J. Phys.: Condens. Matter **33**, 154005 (2021).

[35] J. J. Kas, F. D. Vila, T. S. Tan, and J. J. Rehr, Phys. Chem. Chem. Phys. **24**, 13461 (2022).

[36] B. Helmich-Paris, Int. J. Quantum Chem. **121**, e26559 (2021).

[37] F. D. Vila, J. J. Rehr, H. H. Rossner, and H. J. Krappe, Phys. Rev. B **76**, 014301 (2007).

[38] M. Laraia, C. Hansen, N. R. Shaffer, D. Saumon, D. P. Kilcrease, and C. E. Starrett, High Energy Density Phys. **40**, 100940 (2021).

[39] See https://doi.org/10.17863/CAM.96377 to access the structures and spectra contained in this manuscript.